Journal of Power Sources 294 (2015) 159–166

Contents lists available at ScienceDirect

Journal of Power Sources

journal homepage: www.elsevier.com/locate/jpowsour

# A simple technique for measuring the fracture energy of lithiated thin-film silicon electrodes at various lithium concentrations

Yong Seok Choi [a, b], Matt Pharr [b], Kyu Hwan Oh [a], Joost J. Vlassak [b, *]

[a] Department of Materials Science and Engineering, Seoul National University, Seoul 151-742, South Korea
[b] School of Engineering and Applied Sciences, Harvard University, Cambridge, MA 02138, USA

## HIGHLIGHTS

- The fracture energy of lithiated Si was measured at various states of charge.
- A bending test was performed to determine the critical strain for crack initiation.
- The elastic modulus decreased from 113 GPa for a-Si to 31.6 GPa for $Li_{3.28}Si$.
- The fracture energies were determined to be 12.0 J $m^{-2}$ (a-Si) and 10.0 J $m^{-2}$ ($Li_{3.28}Si$).

## ARTICLE INFO

*Article history:*
Received 23 March 2015
Received in revised form
30 May 2015
Accepted 8 June 2015
Available online 19 June 2015

*Keywords:*
Lithium ion battery
Silicon
Fracture energy
Bending test

## ABSTRACT

We have measured the fracture energy of lithiated silicon thin-film electrodes as a function of lithium concentration using a bending test. First, silicon thin-films on copper substrates were lithiated to various states of charge. Then, bending tests were performed by deforming the substrate to a pre-defined shape, producing a variation of the curvature along the length of the electrode. The bending tests allow determination of the critical strains at which cracks initiate in the lithiated silicon. Using the substrate curvature technique, we also measured the elastic moduli and the stresses that develop in the electrodes during electrochemical lithiation. From these measurements, the fracture energy was calculated as a function of lithium concentration using a finite element simulation of fracture of an elastic–plastic substrate. The fracture energy was determined to be $\Gamma = 12.0 \pm 3.0$ J $m^{-2}$ for amorphous silicon and $\Gamma = 10.0 \pm 3.6$ J $m^{-2}$ for $Li_{3.28}Si$, with little variation in the fracture energy for intermediate Li concentrations. These results provide a guideline for the practical design of high-capacity lithium ion batteries to avoid fracture. The experimental technique described in this paper also provides a simple means of measuring the fracture energy of brittle thin-films.



## 1. Introduction

Lithium ion batteries have been developed to power an increasingly diverse range of applications, such as portable electronic devices and electric vehicles [1–4]. Silicon is considered one of the best candidates as an anode material for the next generation of lithium ion batteries due to its enormous capacity of 3579 mAh $g^{-1}$ ($Li_{15}Si_4$) compared to that of graphite (372 mAh $g^{-1}$), which is currently the anode of choice [5–8]. However, lithium ion insertion and extraction results in a 200–300% increase in volume, which can lead to fracture of the silicon anode during electrochemical cycling [9,10]. Since fracture of the anode can cause a loss of electrical contact and the creation of more surface area for solid electrolyte interphase (SEI) growth, mechanical stability is a key issue in commercial battery applications [11–15].

A number of studies have reported mechanical properties of silicon electrodes. Mönig and colleagues [16,17] investigated the elastic modulus of lithiated silicon nanowires by uniaxial tensile testing. Hertzberg et al. [18] measured the hardness and the elastic modulus of lithiated silicon films using depth-sensing indentation measurements. They found that the hardness decreases from 5 to 1.5 GPa and that the elastic modulus decreases from 92 to 12 GPa in changing from the as-deposited silicon to the fully lithiated silicon ($Li_{15}Si_4$). Also, Sethuraman et al. [19] performed *in-situ* stress measurements of thin-film silicon electrodes using the substrate-curvature technique, finding a biaxial elastic modulus of 70 GPa

* Corresponding author.
*E-mail address:* Vlassak@seas.harvard.edu (J.J. Vlassak).

http://dx.doi.org/10.1016/j.jpowsour.2015.06.063
0378-7753/

for $Li_{0.32}Si$ and 35 GPa for $Li_{3.0}Si$. Pharr et al. [20] evaluated the fracture energy Γ of lithiated silicon by monitoring the stress and morphological development of cracks during electrochemical cycling. They measured a fracture energy of 8.5 ± 4.3 J m$^{-2}$ at small concentrations of lithium (~$Li_{0.7}Si$), and established bounds of 5.4 ± 2.2 J m$^{-2}$ to 6.9 ± 1.9 J m$^{-2}$ for $\Gamma$ at large concentrations of lithium (~$Li_{2.8}Si$). In addition, Nadimpalli et al. [21] estimated an upper bound of 9–11 J m$^{-2}$ for the fracture energy of $Li_{0.4}Si$ based on stress data and electron microscopy observations. However, these measurement techniques have limitations due to the difficulty of determining the critical stress at which cracks initiate on the surface of the electrode. Furthermore, experimental measurements of fracture energy over a range of lithium concentrations are lacking. In order to design durable silicon electrodes, it is essential to know the fracture energy as a function of state of charge.

In this study, we introduce a simple technique for measuring the fracture energy of thin-film silicon electrodes as a function of lithium concentration. We first lithiate amorphous silicon (a-Si) thin-film electrodes on copper substrates to different states of charge. We then perform a bending test by deforming the substrate to a pre-defined shape that allows for a variation in the curvature along the length of the sample. After bending, the electrodes are examined using a focused ion beam (FIB) to obtain both the critical strain for crack initiation and the thickness of the electrodes after lithiation. Using the substrate curvature technique, we measure both the elastic modulus of the lithiated silicon and the stress induced by lithiation. Combining these results, we quantify the fracture energy using a fracture mechanics analysis. The simple technique presented here is not only useful for lithiated-silicon thin-film electrodes but is also generally applicable for measuring the fracture energy of thin-films and coatings.

## 2. Experimental procedures

All electrochemical measurements were performed using a standard three-electrode configuration in a custom-fabricated, hermetic, Teflon cell with a glass window. Both the reference and counter electrodes consisted of lithium foil, while the working electrode was a thin-film of amorphous silicon on a copper substrate (McMaster-Carr, annealed electrolytic tough pitch copper). To fabricate the working electrode, mechanically polished copper substrates (10 mm × 70 mm) with a thickness of 0.8 mm were electro-polished (2 V, 15 min) in phosphoric acid (85 wt%) and placed in a sputter deposition system (ATC 1800, AJA Int., Scituate). Immediately before deposition, the substrates were plasma cleaned for 5 min in 20 mTorr of argon using an RF power of 24 W. Then, 20 nm of copper was deposited onto the substrates using an argon working pressure of 5 mTorr and a DC power of 200 W. The purpose of this copper film was to provide a fresh surface for silicon film deposition. The silicon film was then deposited directly onto the copper film using an argon pressure of 5 mTorr and a DC power of 100 W. The working area of each silicon electrode was 10 mm × 35 mm, and the silicon electrode thickness was 550 ± 15 nm.

The electrolyte consisted of a 1 M solution of $LiPF_6$ in 1:1:1 (wt%) ethylene carbonate:diethyl carbonate:dimethyl carbonate. The electrochemical cells were assembled in a glove box in an ultrahigh purity argon atmosphere with a moisture content of less than 0.1 ppm. Electrochemical measurements were performed with a VersaSTAT 3 galvanostat from Princeton Applied Research. The silicon electrodes were lithiated at a constant current density of 100 μA cm$^{-2}$ (a C/16 rate assuming a capacity of 3579 mAh g$^{-1}$), and then potentiostatically held until the current dropped to less than 4% of its original value to reach diffusive equilibrium at four different states of charge: 1/4 (895 mAh g$^{-1}$), 1/2 (1790 mAh g$^{-1}$), 3/4 (2684 mAh g$^{-1}$), and full (3579 mAh g$^{-1}$). All lithiation processes were conducted within a voltage window of 0.05–3.0 V. After lithiation, the electrodes were removed from the cell, rinsed in dimethyl carbonate (DMC), and dried for 5 min inside the glove box.

Bending tests on the working electrodes were performed inside the glove box 15 min after removing the electrodes from the cell. The tests were performed using a Delrin mandrel (Fig. 1a) that consisted of a male and a female part. The female part had the shape of an ellipsoid, described in x-y coordinates by $9x^2 + y^2 = 9$ (cm), to impose a variable curvature along the length of the sample; the male part had a similar shape, accounting for sample thickness. The strain in the surface of the substrate is then given by [22]:

$$\varepsilon = \frac{h_{sub}}{2\rho}, \tag{1}$$

where $h_{sub}$ is the thickness of substrate and $\rho$ is the local radius of curvature of the substrate. The strain imposed on the electrode film is tensile and varies from 11% in the center of the sample to 0.9% at the edge, as illustrated in Fig. 1b. Prior to bending, the silicon electrodes were scratched with a diamond scribe to introduce imperfections with sizes on the order of the film thickness [20]. Also, marks were drawn at 1 mm increments along the specimen to quantify the position of crack initiation. Then, the samples were placed between the male and female parts of the mandrel and deformed to the shape of the mandrel. Two sets of samples were tested under identical conditions to examine the reproducibility of the experiments. The mandrels are quite stiff, which ensures reproducible deformation of the sample as long as it is in full contact with the surfaces of the mandrel. After the bending test, the samples were sealed in an airtight container inside the glove box and immediately transferred to a focused ion beam (FIB, Zeiss NVision 40) chamber to examine the electrode surfaces. During transfer, the samples were exposed to air for less than 30 s. The elastic modulus of the pure silicon film was measured by performing nano-indentation tests using a Hysitron Tribolab nano-indentation system. Indentation tests were performed in load control at a constant loading rate of 200 μN s$^{-1}$. A total of 25 indentations were made in a 5 × 5 array with a spacing of 5 μm between the indentations.

## 3. Results and discussion

Since the silicon thin-film electrodes are constrained in the plane of the film by the relatively thick substrate, lithium insertion is accommodated entirely by expansion of the electrodes in the thickness direction. Thus, it is reasonable to take the thickness of the film, $h_f$, to be linear in the state of charge,

$$h_f = h_o(1 + \beta s), \tag{2}$$

where $h_o$ is the initial thickness of the film, $\beta$ is related to the atomic volumes (Ω) of silicon and the lithiated phase by $\beta = (\Omega_{Li3.75Si} - \Omega_{Si})/\Omega_{Si} = 2.8$ (silicon undergoes a 280% increase in volume when it is fully lithiated), and $s$ is the state of charge of the electrode, with a value of 0 representing pure silicon and a value of 1 representing the fully lithiated state (assumed to be $Li_{3.75}Si$ with a capacity of 3579 mAh g$^{-1}$) [20,23]. It should be noted, however, that SEI formation consumes lithium and thus affects both the thickness of the film and the apparent state of charge [11,24]. In order to examine the effects of SEI formation, we measured the thickness of $Li_xSi$ after different lithiation times using FIB cross-sectioning. Fig. 2 shows the thickness of a $Li_xSi$ thin-film as a function of time for a constant charge rate. The initial thickness of the amorphous silicon

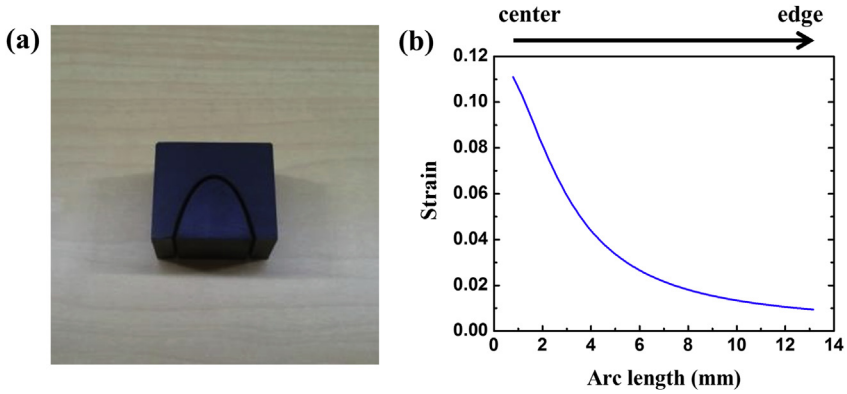


**Fig. 1.** (a) Photograph of the mandrel used for the bending tests. (b) Calculated strain as a function of the position from the center of the sample.

is 550 nm. The black squares represent the expected thicknesses determined using Equation (2) and the state of charge calculated from the lithiation time; the red circles represent the average thicknesses measured by FIB observation. Interestingly, the measured thickness of the silicon electrode is very nearly constant for 2 h and then increases linearly with lithiation time. This observation suggests that most of the lithium inserted during the initial 2 h of the lithiation process was actually used in forming SEI, as opposed to forming the lithiated silicon phase. The observation also suggests that relatively little lithium was used in forming SEI after this initial stage. It is likely that a similar phenomenon occurs in other experimental studies. Thus, this result stresses the need for exercising caution in directly relating the lithiation time to the state of charge in experimental studies. Correspondingly, in this study, we determine the states of charge not from the lithiation time, but based on measurements of the silicon electrode thickness.

The critical strain for fracturing a lithiated silicon electrode can be determined from bending experiments on the electrodes. During bending, small flaws in the lithiated silicon start to grow and propagate in regions where the energy release rate reaches the fracture energy of the lithiated silicon. Thus, the boundary between the cracked and un-cracked regions of the sample provides a measurement of the critical applied strain, $\varepsilon_c$, for fracture. (Shown in Table 1.) Fig. 3(a)–(c) show surface images of a lithiated silicon sample ($Li_{1.4}Si$) after a bending test. The cracks propagate in the transverse direction of the sample, and the crack density near the center of the sample (Fig. 3(a)) is larger than near the edge of the sample (Fig. 3(c)). Fig. 3(d) shows a cross-section of a crack near the boundary between the cracked and un-cracked regions of the sample. Although the sample was lithiated for 8 h, the thickness of the lithiated silicon was 1135 nm, which is approximately 200 nm thinner than the value calculated from Equation (2). This provides clear evidence that lithium is used in the formation of the SEI in the initial lithiation stage. The faces of the cracks appear quite flat and perpendicular to the substrate, suggesting brittle fracture. In addition, the crack opening is quite narrow and there is no evidence of sliding at the interface between the lithiated silicon and copper; any such effects are thereby neglected in these experiments [25,26]. The applied critical strain by itself does not provide sufficient information to evaluate the fracture toughness of the coating. In particular, the energy release rate that drives crack propagation depends on the total stress developed in the film prior to fracture. This total stress can be calculated from the critical bending strain, and from knowledge of the elastic modulus of the film and the stress that develops in the film prior to the bending experiment (i.e., from lithiation).

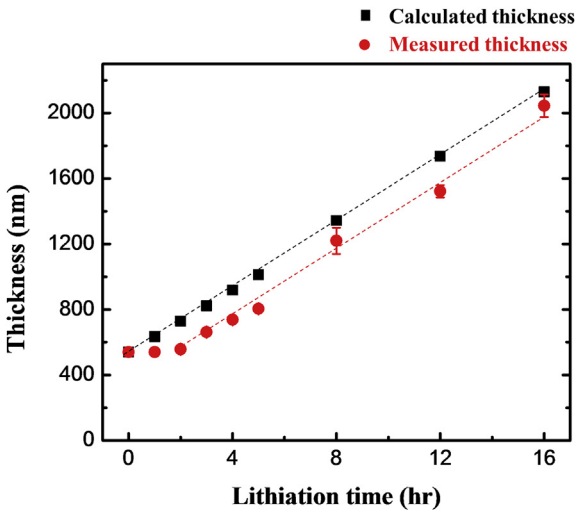


**Fig. 2.** Thickness of a thin-film silicon electrode as a function of the lithiation time at a constant charge rate of C/16. The initial thickness of the silicon electrode is 550 nm. The black squares are values calculated from Equation (2), and the red circles are values measured by a FIB cross-section. (For interpretation of the references to color in this figure legend, the reader is referred to the web version of this article.)

To determine the elastic modulus and the stress at different states of charge, we performed additional electrochemical experiments using 142 nm silicon films on glass substrates (0.4 mm) as anodes. These anodes contained a 300 nm copper film between the silicon and the substrate as a current collector; 20 nm of titanium was used as an adhesion layer between the substrate and the current collector. Three sets of samples were tested under identical conditions. The stress in the lithiated silicon film was determined by measuring the curvature of the substrate with an *in-situ* multi-beam optical sensor (K-Space Associates, Inc.) during lithiation/delithiation. Details of the experimental method have been published in a previous paper [20]. The average stress in the film was then deduced from the substrate curvature using Stoney's equation [20,27,28]:

$$\sigma = \sigma_r + \frac{E_s h_s^2}{6h_f(1-\nu_s)}\Delta K, \tag{3}$$

where $\sigma$ is the average stress in the film, $\sigma_r$ is the residual stress in the as-deposited silicon film, $E_s$ is the elastic modulus of the substrate, $h_s$ is the thickness of the substrate, $\nu_s$ is Poisson's ratio of the substrate, and $\Delta K$ is the change in substrate curvature induced by changes in the film stress. The value of the residual stress in the as-

**Table 1**
Experimental parameters and results as a function of lithium concentration.

| x in $Li_xSi$ | 0 | 0.47 | 1.4 | 2.34 | 3.28 |
|---|---|---|---|---|---|
| Thickness (nm) | 142 ± 1 | 770 ± 20 | 1220 ± 80 | 1523 ± 38 | 2044 ± 70 |
| Poisson's ratio | 0.28 | 0.27 | 0.27 | 0.26 | 0.25 |
| Critical bending strain (%) | 1.35 ± 0.17 | 1.75 ± 0.03 | 1.85 ± 0.05 | 1.91 ± 0.01 | 1.94 ± 0.01 |
| Elastic modulus (GPa) | 113 ± 4.1 | 58.5 ± 6.4 | 49.6 ± 3.7 | 42.9 ± 1.4 | 31.6 ± 2.0 |
| Flow stress (GPa) | +0.045[a] | −0.80 ± 0.05 | −0.54 ± 0.02 | −0.46 ± 0.02 | −0.34 ± 0.04 |
| Relaxation stress (MPa) | 0 | 97 ± 2 | 68 ± 2.4 | 53 ± 1.5 | 45 ± 2.6 |
| Critical stress for fracture (MPa) | 1469 ± 187 | 252 ± 117 | 384 ± 69 | 357 ± 31 | 276 ± 51 |
| pre-factor Z | 4.80 | 3.02 | 2.74 | 2.56 | 2.15 |
| Fracture energy (J $m^{-2}$) | 12.0 ± 3.0 | 2.3 ± 2.2 | 9.2 ± 3.3 | 10.8 ± 1.9 | 10.0 ± 3.6 |

[a] For unlithiated silicon the relevant stress is the residual stress after deposition, not the flow stress.

deposited silicon film, $\sigma_r = 45$ MPa, was determined by measuring the curvature of the glass substrate before and after silicon deposition. In the calculations, values of $E_s = 72$ GPa, and $\nu_s = 0.23$ were used for the glass substrate [29].

Fig. 4(a) and (b) show representative responses of the potential and stress during lithiation and delithiation. In Fig. 4(a), we observe a short plateau around 0.45 V at the beginning of the voltage profile. The time for the initial plateau and the next drop is approximately 1.5 h, which is comparable to the time for SEI formation determined from the electrode thickness measurements. Then, the voltage gradually decreases as the state of charge increases. This sloping voltage profile indicates a single-phase reaction given the slow rate (C/16) used in the experiments. As shown in Fig. 4(b), the stress in the electrode becomes compressive as lithium is inserted until it reaches a value of −1.12 GPa. At that point, the electrode material flows plastically with a continuous reduction in stress as the lithium concentration increases. The stress in the electrode is then equal to the flow stress ($\sigma_{flow}$) of lithiated silicon, independent of the nature of the substrate [30]. During lithiation, the electrodes were delithiated for 10 min at various states of charge ($Li_{0.47}Si$, $Li_{1.4}Si$, $Li_{2.34}Si$, and $Li_{3.28}Si$). During these delithiation segments, the elastic modulus of the lithiated silicon was determined by measuring the change in stress in the electrode, as has been done in previous studies [19,20]. The elastic modulus of the electrode film, $E_f$, is given by [20]:

$$E_f = -3\frac{1+\beta s}{\beta}\frac{\Delta\sigma}{\Delta s}\left(1-\nu_f\right), \tag{4}$$

where $\nu_f$ is Poisson's ratio of the electrode [31] and $\Delta\sigma/\Delta s$ is the increment of the stress over a sufficiently small change of the state of charge. Fig. 4(c) shows the elastic modulus at different states of charge. Our experimental data are designated with red star symbols. The values are averages of three individual experiments; the value for pure amorphous silicon was determined using nanoindentation. Evidently the elastic modulus has decreased significantly at low lithium concentrations (x = 0.47), indicating that even a small amount of lithium affects the properties of the silicon electrode strongly. Further increases in lithium concentration lead to a more gradual decrease of the stiffness. Previously, Hertzberg et al. [18] reported that the elastic modulus decreases from 92 GPa (pure silicon) to 12 GPa (fully lithiated silicon). Furthermore, Sethuraman et al. [19] measured an elastic modulus of 51 GPa for $Li_{0.32}Si$ and 26 GPa for $Li_{3.0}Si$, and Ratchford et al. [32] reported an elastic modulus of ~35 GPa for fully lithiated silicon. All previous and our work suggest that lithium insertion into silicon causes an elastic softening of silicon. However, the numerical values of the moduli are slightly different among the different experiments, most likely due to the use of a different measurement technique [18,32] or reference state [19] for calculating the moduli.

Bending tests were performed on the lithiated electrodes

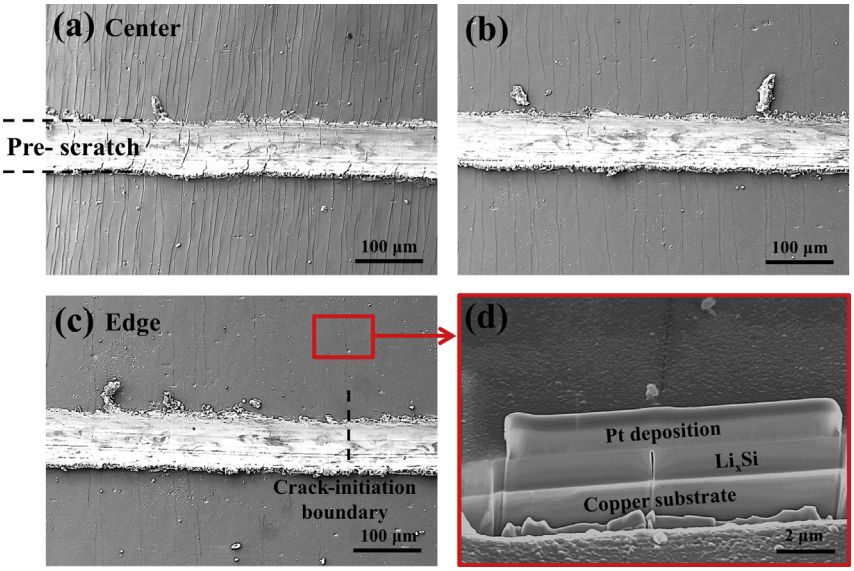


**Fig. 3.** SEM images of cracks after a bending test ($Li_{1.4}Si$). The distance (arc length) from the center of the sample is (a) 2 mm, (b) 6 mm, and (c) 8 mm. (d) Cross-section of the crack in Fig. 3(c) (Tilt angle = 54°). The thickness of $Li_{1.4}Si$ is determined to be 1135 nm.

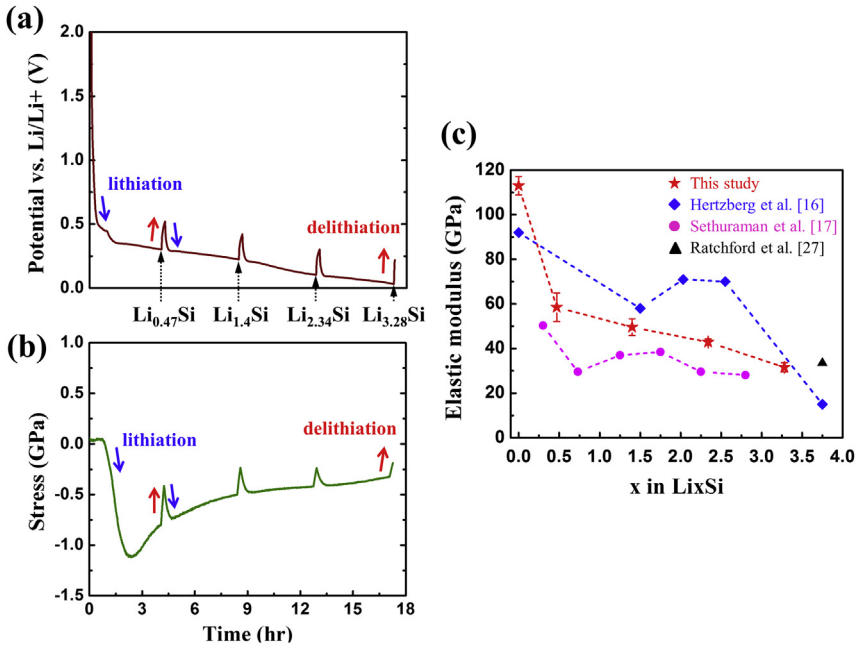


**Fig. 4.** Representative responses in (a) potential vs Li/Li+ and (b) stress as a function of lithiation time during a galvanostatic test of a 142 nm amorphous silicon film. (c) Elastic modulus and flow stress after lithiation of the film as a function of lithium concentration.

exactly 15 min after lithiation. Several researchers have reported rapid stress relaxation in silicon electrodes upon current interruption [19,33,34]. As the driving force for fracture scales with the square of the stress (Equation (6)), even a small amount of stress relaxation can affect the calculation of the fracture energy significantly. Therefore, we measured the relaxation stress ($\sigma_{relax}$) in the electrodes after current interruption. Fig. 5(a) and (b) show representative responses of the potential and stress during lithiation and open-circuit segments for a 142 nm amorphous silicon electrode. As shown in Fig. 5(b), the stress continuously decreases in absolute value during the open-circuit segments. This stress relaxation is quantitatively consistent with previous reports [34] and may be attributed to the high mobility of lithium atoms, which facilitates effective bond switching to accommodate mechanical deformation [35]. The amount of stress relaxation after 15 min of open circuit is plotted in Fig. 5(c).

Fracture of the electrode occurs in the form of long channel cracks in the lithiated silicon film. The energy release rate or driving force for this type of cracks can be calculated using an analysis by Beuth for cracks in a thin-film on an elastic half space [36,37]. Pharr

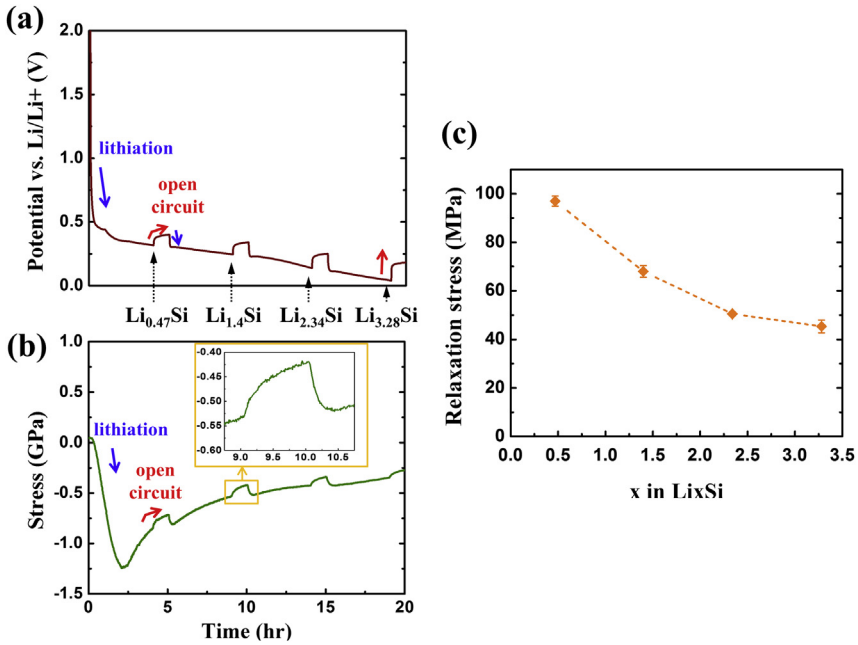


**Fig. 5.** Representative responses in (a) potential vs Li/Li+ and (b) stress as a function of lithiation time from a galvanostatic test of a 142 nm amorphous silicon film. (c) Relaxation stress of silicon film after 15 min of open circuit as a function of lithium concentration.

et al. [20] have discussed in detail the validity of such an analysis in this context. However, one concern with Beuth's analysis is the assumption of an elastic substrate, which is clearly violated in our bending experiments on copper substrates. To evaluate the impact of substrate plasticity on the calculation of the fracture energy, we performed finite element analyses of the energy release rate in the presence of substrate plasticity. For the lithiated film, the elastic moduli used in the analyses were extracted from the electrochemical experiments, as shown in Table 1. Poisson's ratios of $Li_xSi$ were taken from atomistic simulations performed by Shenoy et al. [31], also shown in Table 1. The film was modeled as elastic since the critical stresses to cause fracture were found to be less than the yield strength of amorphous $Li_xSi$ in all of our fracture experiments. The copper substrate was modeled as elastic–plastic. The stress-strain behavior of the substrate was measured following the ASTM-E8M standard. From the tensile tests, the modulus was found to be $E_s = 117$ GPa, and the yield strength $\sigma_s^Y = 260$ MPa. A typical value for Poisson's ratio for copper of $\nu_s = 0.35$ was used in the simulations. The yield stress of the copper was directly prescribed in ABAQUS as a function of the plastic strain based on the experimental stress-strain curves, and isotropic hardening was assumed. Large deformation was enabled during the entire simulation. Both the film and the substrate were assumed to be isotropic. Four node bilinear plane strain quadrilateral elements with reduced integration (CPE4R) were implemented to model the cracking process as plane strain.

The geometry (cross-section view) of the simulation is shown in Fig. 6. Only half of the geometry was modeled due to symmetry, and only the region of the substrate near the film/substrate interface was modeled because the copper substrate was much thicker than the film. Increasing the thickness of the substrate did not affect the results. Prior to bending, the substrate was stress-free because it is much thicker than the film; the film was under a state of equal biaxial compression equal to the flow stress minus the relaxation stress (Table 1). This state of stress was imposed in ABAQUS by using the predefined-field function during the initial step (Fig. 6a). In the experiments, the electrodes were then subjected to a state of bending, as previously described. Due to this bending, the substrate near the film/substrate interface is essentially under a state of uniaxial tension. Correspondingly, to simulate bending, a displacement was imposed on the right edge of the film/substrate (Fig. 6b). The system was incrementally loaded in ABAQUS until it reached the critical strain for a given lithium concentration (Table 1). Next, a cut was created through the thickness of the film at the left edge of the geometry (Fig. 6c), which represented a steady-state channel crack. Initially, a traction was applied on the cut that was equal and opposite to the stress in the film, and the film behaved as if it is not cracked. Incrementally, this traction was reduced to zero, and the crack opened. During cracking, the stress in the film far from the crack remained constant.

From this simulation, we were able to calculate the energy release rate in a manner similar to that of Beuth [36]. In particular, in the steady-state, the energy release rate is equal to the energy released by converting a unit length of un-cracked film far ahead of the crack tip to a unit length of cracked material (i.e. the final state in our simulation) far behind the crack tip. In other words, the steady-state energy release rate is related to the change in internal energy upon introducing the crack. The internal energy, $U$, is computed in ABAQUS and includes the recoverable strain energy as well as the energy dissipated by plastic deformation in the substrate. As the crack opens, the recoverable strain energy decreases, while the energy dissipated in plasticity increases. The energy available for fracture of the film, i.e., the energy release rate, is then related to these energies by:

$$G = \frac{2(U_{no-crack} - U_{crack})}{h_f}, \tag{5}$$

where $h_f$ is the thickness of the film, $U_{no-crack}$ represents the internal energy of the system just before the crack is introduced, and $U_{crack}$ represents the internal energy of the system at the end of the simulation. The factor of two in Equation (5) arises since only half of the geometry was simulated. Following standard practice, the pre-factor $Z$ is then calculated through:

$$G = \frac{Z\sigma_f^2 h_f}{\bar{E}_f}, \tag{6}$$

where $\sigma_f$ is the critical total stress in the film to cause cracking, and $\bar{E}_f = E_f/(1-\nu_f^2)$ is the plane-strain modulus of the film, where $\nu_f$ is Poisson's ratio of the film.

Combining (5) and (6) yields:

$$Z = \frac{2\bar{E}_f(U_{no-crack} - U_{crack})}{\sigma_f^2 h_f^2}. \tag{7}$$

This approach was verified in ABAQUS by making the substrate elastic and comparing to Beuth's results for a number of geometries and materials constants (results not shown here) [36]. The results from ABAQUS were in agreement with the results obtained by Beuth to within 5–10 %. Using this approach, the pre-factor $Z$ was found as a function of the lithium concentration and is tabulated in Table 1.

At the critical bending strain to induce fracture, $G=\Gamma$ and Equation (6) can be used to find the fracture energy. Since the critical bending strains (Table 1) are much larger than the yield strain of Cu (approximately 0.3%), we assume that plastic deformation in the substrate occurs during the entire bending experiment, i.e., effectively, $\nu_s = 0.5$. During bending and prior to fracture, the film is under a state of plane stress. Assuming continuity at the interface between the film and the substrate, the change in stress in

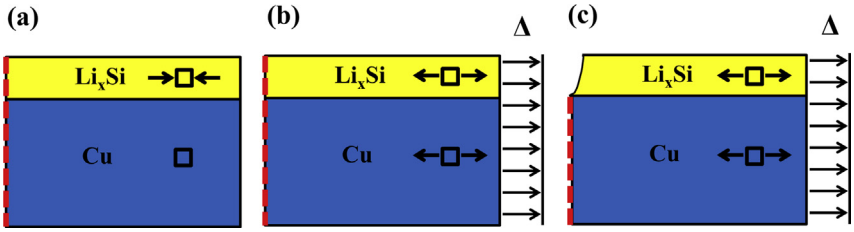


**Fig. 6.** An illustration (cross-section view) of the ABAQUS simulation to calculate the fracture energy. The dotted lines represent sections with mirror symmetry. (a) A predefined field (equal biaxial compression) is prescribed in the film to represent the stress due to sputtering, lithiation, and "relaxation." (b) A displacement is applied to the right edge of the film and substrate to represent the bending-induced strain prior to fracture. (c) A channel crack is introduced into the film.

the film due to bending can be found from Hooke's law:

$$\varepsilon_{11}^{bend} = \frac{1}{E_f}\left[\sigma_{11}^{bend} - \nu_f \sigma_{22}^{bend}\right] = \varepsilon_c, \tag{8}$$

$$\varepsilon_{22}^{bend} = \frac{1}{E_f}\left[\sigma_{22}^{bend} - \nu_f \sigma_{11}^{bend}\right] = \nu_s \varepsilon_c, \tag{9}$$

where $\varepsilon_c$ is the critical bending strain to cause fracture (Table 1). The subscripts 1 and 2 refer to the directions parallel and perpendicular to the long edge of the sample, respectively.

Combining (8) and (9) gives the bending stress ($\sigma_b$):

$$\sigma_b = \sigma_{11}^{bend} = E_f \varepsilon_c \left[\frac{1 - \nu_f \nu_s}{1 - \nu_f^2}\right]. \tag{10}$$

Using $\nu_s = 0.5$, and $\nu_f$, $E_f$, and $\varepsilon_c$ from Table 1, the critical stress for fracture (summation of $\sigma_b$, $\sigma_{flow}$, and $\sigma_{relax}$) is calculated from Equation (10) and is listed in Table 1. With the critical stress known, we can use Equation (6) to calculate the fracture energy – the results are shown in Table 1 and Fig. 7. The fracture energy of the pure silicon film is $\Gamma = 12.0 \pm 3.0$ J m$^{-2}$. Although the lithium concentration of the electrode increases to $Li_{3.28}Si$, the fracture energy remains similar ($\Gamma = 10.0 \pm 3.6$ J m$^{-2}$) to that of pure silicon. These fracture energies are quite typical for brittle solids, in agreement with the observation of brittle fracture morphologies in the bending experiments (Fig. 3). The values of the fracture energy do not change much with lithium concentration, even though the stiffness of the coatings changes dramatically. The one exception is the fracture energy of $Li_{0.47}Si$, which is significantly lower than the other values. Part of this reduction may be explained by the error associated with the stress measurement. In particular, the stresses measured may be inaccurate at these small lithium concentrations because the stress state varies rapidly at the onset of lithiation. However, the error in the stress measurement alone is not sufficient to explain the low value of the fracture energy and it is possible that the fracture energy goes through a minimum near this lithium concentration. Previously, Pharr et al. [20] have reported a fracture energy for lithiated silicon of 8.5 ± 4.3 J m$^{-2}$ at low concentrations of lithium (~$Li_{0.7}Si$), and established bounds of 5.4 ± 2.2 J m$^{-2}$ to 6.9 ± 1.9 J m$^{-2}$ at large concentrations of lithium (~$Li_{2.8}Si$). These values are in reasonable agreement with the fracture energies measured in this study: 9.2 ± 3.3 J m$^{-2}$ at $Li_{1.4}Si$ and 10.8 ± 1.9 J m$^{-2}$ at $Li_{2.34}Si$. The small discrepancy may be caused by the history dependence of the plastic flow that occurs in the substrate during crack growth: As the crack propagates, the precise strain history in the ABAQUS model may be slightly different from the actual strain history. The energy dissipated in the substrate during crack growth is then slightly different from the calculated value, leading to a small error in the energy release rate calculated by ABAQUS.

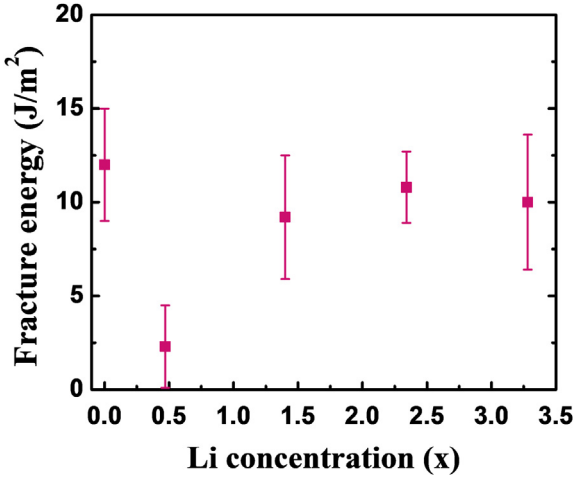


**Fig. 7.** Fracture energy as a function of lithium concentration calculated from Equation (6).

The technique for measuring fracture energy described in this paper offers a number of important advantages over existing techniques. Since the critical bending strain at which the crack initiates is readily determined after the experiment by optical or electron microscopy, more accurate values of fracture energy can be obtained as compared to other techniques [20,21]. Also, customizing the shape of the mandrel allows for a variation in the curvature along the length of the sample that can be prescribed by the user, thereby providing a means of controlling the range of the applied strain. Thus, it is possible to observe a large range of prescribed strains from a single experiment.

## 4. Conclusion

In this paper, we have determined the fracture energy of lithiated silicon thin-film electrodes at various states of charge. To do so, we performed a simple bending test by deforming the substrate to a customized shape. The states of charge were determined by measuring the thickness of the lithiated silicon electrode, since most of the lithium inserted during the initial stage of the experiment was consumed in forming SEI. Using the substrate curvature technique, the elastic moduli of the electrodes were calculated as a function of lithium concentration, varying from 113 GPa for amorphous silicon to 31.6 GPa for $Li_{3.28}Si$. In addition, the total critical stress for fracture in the silicon electrodes was found by measuring stresses due to lithiation, relaxation, and bending. From this total critical stress, we quantified the fracture energy through simulations in ABAQUS of an elastic film on an elastic–plastic substrate. The fracture energies were determined to be $\Gamma = 12.0 \pm 3.0$ J m$^{-2}$ for amorphous silicon and $\Gamma = 10.0 \pm 3.6$ J m$^{-2}$ for $Li_{3.28}Si$, with little variation in the fracture energy for intermediate Li concentrations. We believe that the simple technique presented here will be useful for measuring the fracture energy of a wide range of thin-films and coatings.

## Acknowledgments

This work was supported by the National Science Foundation through a grant on Lithium-ion Batteries (CMMI-1031161). It was performed in part at the Center for Nanoscale Systems, a member of the National Nanotechnology Infrastructure Network, which is supported by the National Science Foundation under NSF Award No. ECS-0335765, and at the Harvard University Materials Research Science and Engineering Center, which is supported by the National Science Foundation under Award No. DMR 14-20570. M.P. acknowledges support by the National Science Foundation Graduate Research Fellowship Program. Work at Seoul National University was supported by a grant from the Fundamental R&D Program for Technology of World Premier Materials funded by the Ministry of Knowledge Economy, Republic of Korea (10037919).

## References

[1] M. Armand, J.-M. Tarascon, Nature 451 (2008) 652–657.
[2] J.-M. Tarascon, M. Armand, Nature 414 (2001) 359–367.
[3] R. Marom, S.F. Amalraj, N. Leifer, D. Jacob, D. Aurbach, J. Mater. Chem. 21 (2011) 9938–9954.
[4] M.S. Whittingham, MRS Bull. 33 (2008) 411–419.
[5] M.N. Obrovac, L. Christensen, Electrochem. Solid State Lett. 7 (2004) A93–A96.

[6] J.R. Dahn, T. Zheng, Y. Liu, J.S. Xue, Science 270 (1995) 590–593.
[7] U. Kasavajjula, C. Wang, A.J. Appleby, J. Power Sources 163 (2007) 1003–1039.
[8] S.-B. Son, J.E. Trevey, H. Roh, S.-H. Kim, K.-B. Kim, J.S. Cho, J.-T. Moon, C.M. DeLuca, K.K. Maute, M.L. Dunn, H.N. Han, K.H. Oh, S.-H. Lee, Adv. Energy Mater. 1 (2011) 1199–1204.
[9] L.Y. Beaulieu, K.W. Eberman, R.L. Turner, L.J. Krause, J.R. Dahn, Electrochem. Solid State Lett. 4 (2001) A137–A140.
[10] C.K. Chan, H. Peng, G. Liu, K. Mcllwrath, X.F. Zhang, R.A. Huggins, Y. Cui, Nat. Nanotechnol. 3 (2008) 31–35.
[11] S.P. Nadimpalli, V.A. Sethuraman, S. Dalavi, B. Lucht, M.J. Chon, V.B. Shenoy, P.R. Guduru, J. Power Sources 215 (2012) 145–151.
[12] Y.S. Choi, M. Pharr, C.S. Kang, S.-B. Son, S.C. Kim, K.-B. Kim, H. Roh, S.-H. Lee, K.H. Oh, J.J. Vlassak, J. Power Sources 265 (2014) 160–165.
[13] S.D. Beattie, D. Larcher, M. Morcrette, B. Simon, J.-M. Tarascon, J. Electrochem. Soc. 155 (2008) A158–A163.
[14] R. Deshpande, M. Verbrugge, Y.-T. Cheng, J. Wang, P. Liu, J. Electrochem. Soc. 159 (2012) A1730–A1738.
[15] C.S. Kang, S.-B. Son, J.W. Kim, S.C. Kim, Y.S. Choi, J.Y. Heo, S.-S. Suh, Y.-U. Kim, Y.Y. Chu, J.S. Cho, J. Power Sources 267 (2014) 739–743.
[16] S.T. Boles, A. Sedlmayr, O. Kraft, R. Mönig, Appl. Phys. Lett. 100 (2012) 243901.
[17] S.T. Boles, C.V. Thompson, O. Kraft, R. Mönig, Appl. Phys. Lett. 103 (2013) 263906.
[18] B. Hertzberg, J. Benson, G. Yushin, Electrochem. Commun. 13 (2011) 818–821.
[19] V.A. Sethuraman, M.J. Chon, M. Shimshak, N. Van Winkle, P.R. Guduru, Electrochem. Commun. 12 (2010) 1614–1617.
[20] M. Pharr, Z. Suo, J.J. Vlassak, Nano Lett. 13 (2013) 5570–5577.
[21] S.P. Nadimpalli, V.A. Sethuraman, G. Bucci, V. Srinivasan, A.F. Bower, P.R. Guduru, J. Electrochem. Soc. 160 (2013) A1885–A1893.
[22] F. Beer, E.R Johnston Jr, J.T. DeWolf, D. Mazurek, New York, McGraw-Hills, 2009.
[23] M.N. Obrovac, L.J. Krause, J. Electrochem. Soc. 154 (2007) A103–A108.
[24] M.B. Pinson, M.Z. Bazant, J. Electrochem. Soc. 160 (2013) A243–A250.
[25] X. Xiao, P. Liu, M. Verbrugge, H. Haftbaradaran, H. Gao, J. Power Sources 196 (2011) 1409–1416.
[26] H. Haftbaradaran, X. Xiao, M.W. Verbrugge, H. Gao, J. Power Sources 206 (2012) 357–366.
[27] G.G. Stoney, Proc. R. Soc. Lond. Ser. A 82 (1909) 172–175.
[28] W.D. Nix, Metall. Trans. A 20 (1989) 2217–2245.
[29] Physical properties of clear soda lime float glass provided by manufacturer, Abrisa Technologies, Santa Paula, CA.
[30] K. Zhao, M. Pharr, J.J. Vlassak, Z. Suo, J. Appl. Phys. 109 (2011) 016110.
[31] V. Shenoy, P. Johari, Y. Qj, J. Power Sources 195 (2010) 6825–6830.
[32] J. Ratchford, B. Schuster, B. Crawford, C. Lundgren, J. Allen, J. Wolfenstine, J. Power Sources 196 (2011) 7747–7749.
[33] V.A. Sethuraman, V. Srinivasan, A.F. Bower, P.R. Guduru, J. Electrochem. Soc. 157 (2010) A1253–A1261.
[34] M. Pharr, Z. Suo, J.J. Vlassak, J. Power Sources 270 (2014) 569–575.
[35] S. Huang, T. Zhu, J. Power Sources 196 (2011) 3664–3668.
[36] J. Beuth Jr., Int. J. Solids Struct. 29 (1992) 1657–1675.
[37] T. Nakamura, S.M. Kamath, Mech. Mater. 13 (1992) 67–77.